Electrical characterization of ultra-thin Tungsten films made by novel hotwire-assisted atomic layer deposition

Kees van der Zouw, Antonius A.I. Aarnink, Jurriaan Schmitz, Alexey Y. Kovalgin,
MESA+ Institute for Nanotechnology, University of Twente, P.O. Box 217, 7500 AE, Enschede, The Netherlands
Email: a.y.kovalgin@utwente.nl

***Abstract*—In this work, we applied conventional Van der Pauw and circular transmission line method (CTLM) test structures to determine the sheet and contact resistance of ultra-thin (1-10 nm) tungsten films grown by Hot Wire assisted Atomic Layer Deposition, as well as their temperature coefficient of resistance (TCR). We finally explored the field effect (FE) in these layers.**

***Index Terms*—Thin films, tungsten, atomic layer deposition, spectroscopic ellipsometry, sheet resistance, contact resistance, transfer length, temperature coefficient of resistance, field effect**

I. Introduction

The continuous downscaling of electronic devices poses an increasing demand for the use of ultra-thin films in a variety of applications such as microprocessors, image sensors, memories, and physical unclonable-function devices [1,2]. Both isolating and metallic layers are widely requested. Among a variety of characteristics, film conformality, uniformity, thickness, step coverage and resistivity may be of crucial importance. Tungsten (W) is one of the metals commonly adopted by industry in integrated circuits to realize electrodes and interconnects [3]. With decreasing the film thickness, the main challenge is to keep the sheet and contact resistances low enough, in line with the application demands [4]. Further, the ultra-thin metal films may be expected to exhibit a field effect, which is not observable in the thick layers due to the high electron density and the related screening effect [5-10]. All this makes determining the electrical behavior of ultra-thin W films relevant and important.

Atomic Layer Deposition (ALD) is a deposition technique that perfectly fits with the need for miniaturization. ALD is known to provide high layer uniformity and conformality, together with excellent step-coverage and precise layer-thickness control, due to its attribute of sequential, self-limiting surface reactions [11]. This makes ALD the method of choice for many applications. ALD can be categorized in two main classes: thermal ALD and radical enhanced ALD (REALD). Many single element deposition processes can not be executed in pure thermal mode [11,12]. Radicals help induce reactions which would otherwise not occur. A plasma is often used as a source of radicals. However, there is a number of drawbacks while using a plasma. First, a plasma can damage the wafer. Secondly, multiple reactions take place in plasma: the wafer may be exposed to unwanted radicals, atoms, ions, or UV photons [13]. Recently, we developed a novel approach to ALD, the so-called Hot Wire assisted ALD (HWALD) [14]. A hot wire takes the place of the plasma as the radical source. HWALD has been successfully applied to deposit either α- or β-phase crystalline W, depending on the conditions [15-19].

In this work, we apply conventional Van der Pauw and circular transmission line method (CTLM) test structures to determine the sheet and contact resistance and transfer length of ultra-thin (1-10 nm) W films grown by HWALD, as well as their temperature coefficient of resistance (TCR). We finally explored the field effect (FE) in these layers.

II. Test structure fabrication

Highly doped p-type 4-inch (100) Si wafers were used as substrates (see Fig. 1 for the process flow). Prior to thermal oxidation, the wafers were ozone-steam cleaned, followed by an 1% HF deep for 1 min. Oxidation was carried out at 1100 °C for 45 minutes in dry oxygen, to obtain approximately 100 nm of SiO_2. Protoresist was applied and patterned accordingly to the desired electrode shapes given by the first lithography mask. Sputtering of a 10-nm-thick titanium adhesion layer and 40 nm thick platinum (Pt) layer was followed by a lift-off step to pattern the Pt electrodes. A tungsten film and an a-Si capping layer (to prevent oxidation of the W in air) were deposited by HWALD and chemical vapor deposition (CVD), respectively. Further patterning was performed by a second lithography step, subsequent wet-etching of the W and a-Si layers in a solution containing 0.67% of HF and 50% of HNO_3, and by stripping the photoresist in fuming HNO_3. A new layer of photoresist was spin-coated over the front-side of the wafer, to protect the surface during the back-side SiO_2 removal in buffered HF. Sputtering of a 400-nm-thick aluminum film as the back-side electrode (back gate), to study the field effect, finalized the structures.

The HWALD deposition of W was performed from tungsten-hexafluoride (WF_6) and hydrogen (H_2) precursors at a substrate temperature of 275 °C. The hot-wire dissociates the H_2 into atomic hydrogen (at-H) radicals. A hot-wall reactor

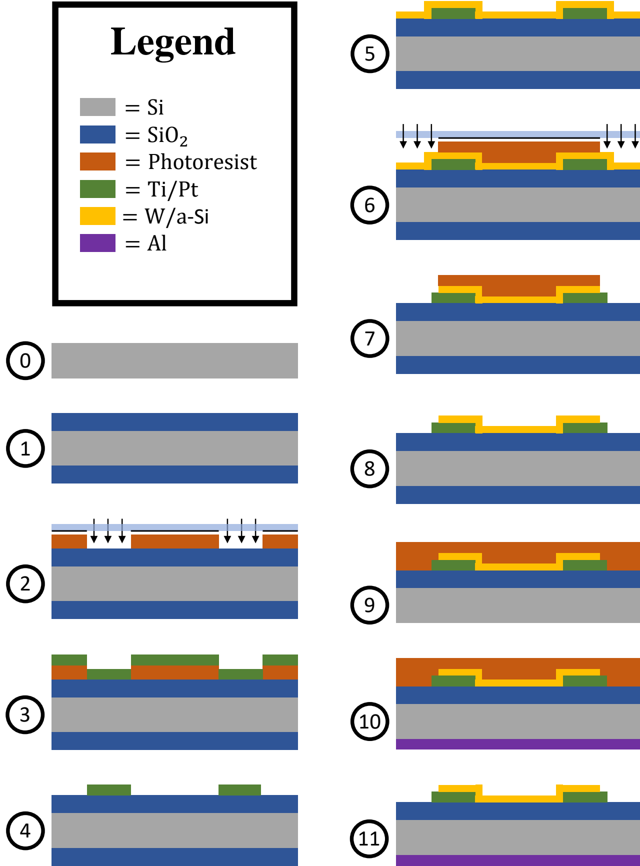

Fig. 1. Schematic of the process flow to fabricate the test structures.

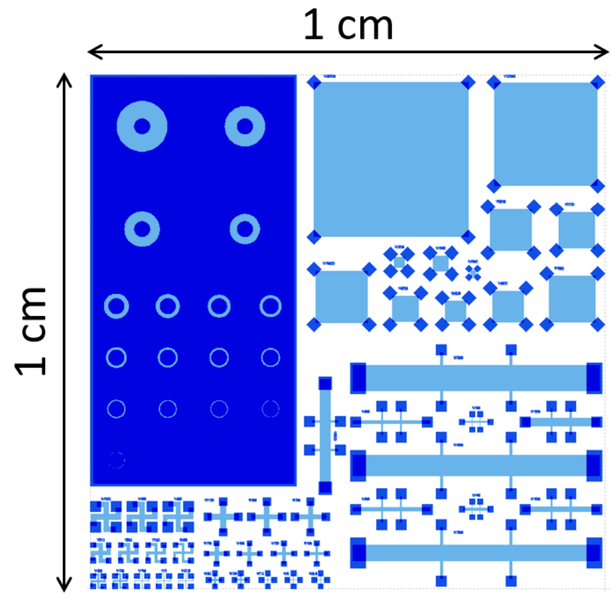

(a)

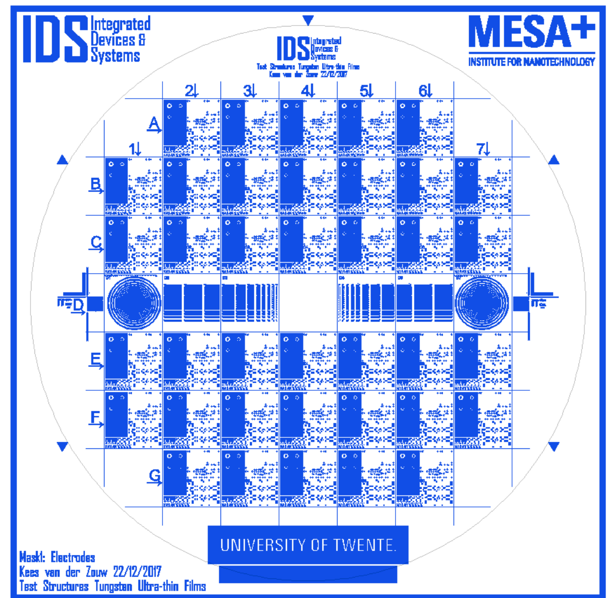

(b)

Fig. 2. (a) The repeating wafer segment with different test structures. (b) The wafer layout including all the segments.

was used to grow low-resistivity α-phase W films [18]. No growth of W was observed on SiO_2 directly [19]. To initiate the HWALD growth of W, a CVD Si seed layer is grown on top of the SiO_2 by dissociation of tri-silane (Si_3H_8), after which it is replaced by a W seed layer by introducing WF_6 into the reactor. Thickness of the HWALD W was monitored in-situ by spectroscopic ellipsometry (SE). The set of thicknesses consisted of 10-, 2.5-, 1.5- and 1.0-nm films measured by SE in the central 1×1 cm^2 area on each wafer.

III. Test Structure Design

Each wafer is subdivided into segments. The segment layout is shown in Fig. 2a. Each segment consists of several Van der Pauw, CTLM, Greek-cross and Hall structures of various dimensions. As shown in Fig. 2b, the segments were evenly distributed across the wafer surface.

For each type of structure, a number of considerations was made in the design process. Only the considerations for the Van der Pauw and CTLM structures will be discussed in detail, since all results presented in this work involve measurements on these structures. The Van der Pauw equation for the sheet resistance holds for the ideal case of infinitesimally small contacts at the circumference of the sample [20,21]. In practice, this condition is not met and a correction factor should be included. The design of the Van der Pauw structures used in this work, is based on and bares close resemblance to the symmetrical octagon analytically treated by [22], due to the fact that the electrodes are positioned at the corners of the structure (see Fig. 3a). Small deviations of the electrode's placement can be expected due to the alignment inaccuracy during fabrication. Further, the transfer length (L_T) should be considered. L_T is the length

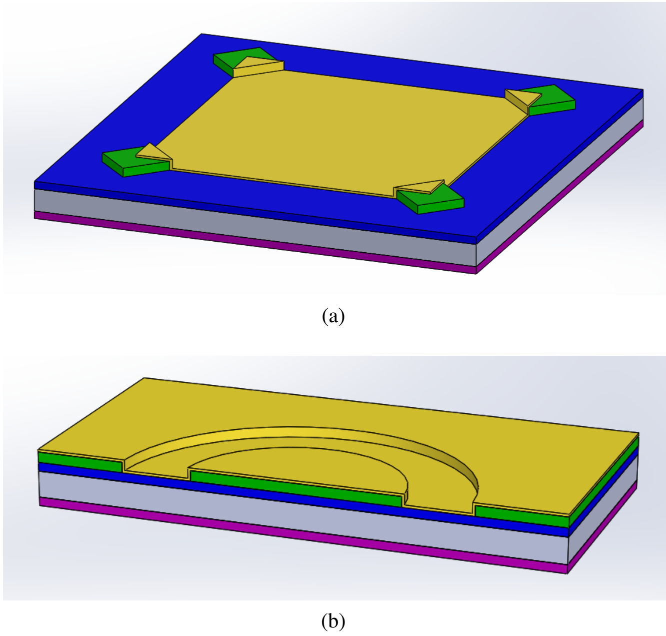

(a)

(b)

Fig. 3. Schematic representation of the typical test structures used in this work. (a) The Van der Pauw structure. (b) the CTLM structure. The dimensions are not to scale.

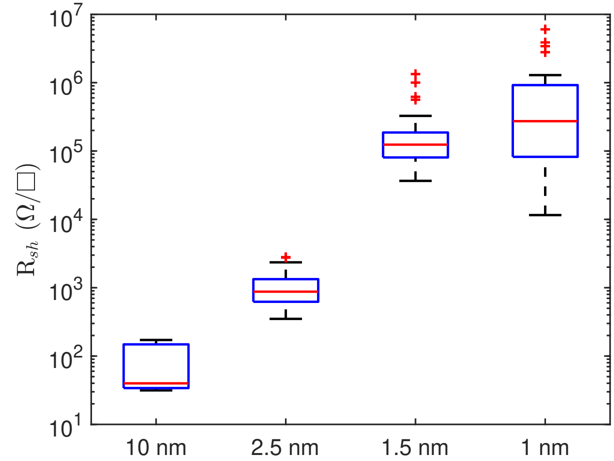

Fig. 4. The sheet-resistance variations across differently thick (as measured in the central 1×1 cm^2 area on each wafer) wafers. The middle-box line indicates the median, the lower and upper edges of each box show the data points statistically falling into the 25% to 75% range, respectively. The error bars indicate the most extreme data excluded from the 25%-75% range but still not classified as outliers. The several outliers are plotted individually using the (+) symbol.

over which the electrical current is transferred between the electrodes and the W sheet. The ratio between contact length and the total length of the structures at the circumference of the structure is kept around 0.1 for each structure, which means that the Van der Pauw equation should hold with high accuracy [22].

The CTLM structures as designed for this work have a circular inner electrode, separated from the outer electrode by a gap W_g (variable), as shown in Fig. 3b. By choosing a radius for the inner electrode (R_{el}) much larger than $4L_T$ and W_g, the values for the sheet resistance (R_{sh}), the contact resistance (R_C) and L_T can be extracted from the corresponding resistance versus W_g plot [23,24]. It is assumed that the electrode resistance is negligible and the sheet resistance on top of the electrodes and within the gap is identical [25,26].

IV. Electrical Measurement Results

A. Sheet resistance

The sheet resistance (R_{sh}) of the W films was measured using Van der Pauw structures. Fig. 4 shows the cumulative R_{sh} plots of the differently-thick W films. It can be seen that R_{sh} increases with decreasing film thickness. Further, significant variations of R_{sh} are obtained across each wafer. For the thinner layers, the variations of R_{sh} are presumably due to small thickness non-uniformity of the W. As has been demonstrated in our earlier work [18,27], R_{sh} of ultra-thin metallic layers can be extremely sensitive to very small thickness variations, even on a sub-nm scale. For the 10-nm-thick W film, the variations of R_{sh} are attributed mainly to a change in W crystallinity across the wafer. The bottom half shows significantly larger R_{sh}, compared to the top half of the wafer. X-ray diffraction (XRD) measurements have been performed to determine the crystal-phases present in the two spatial regimes (see Fig. 5). The tungsten peaks within the measurement range are located at 40.2° [(110) plane], 58.2° [(200) plane] and 73.2° [(211) plane] for α-W [28], and at 35.5° [(002) plane], 39.8° [(012) plane] and 43.8° [(112) plane] for β-W [29,30]. It is difficult to distinguish the peaks around ∼40° due to possible overlap. However, the peaks at 35.5°, 58.2° and 73.2° suggest that the top-half of the wafer contains primarily α-W, while the bottom-half of the wafer contains primarily β-W. The resistivity of the 10-nm-thick α-W is estimated at $\rho = 32\ \mu\Omega \cdot cm$, which is roughly six times larger than the bulk resistivity for α-W (5.6 $\mu\Omega \cdot cm$, [31]) and smaller than the bulk resistivity for β-W (100-1290 $\mu\Omega \cdot cm$, [32-34]).

Due to the difficulty to measure the local (i.e., determining the electrical behavior) film thickness for each individual device, all thin-film properties in the remainder of this work are plotted against the sheet resistance and not the film resistivity.

B. Contact resistance and transfer length

To measure the contact resistance and the transfer length, the CTLM structures with 10-nm- and 2.5-nm-thick HWALD W layers were analysed. From Fig. 6a, one might suggest a slight increase of the R_C with increasing R_{sh}, which can be explained by increased current crowding and quantum confinement in the thinner layers. However, no conclusive observation can yet be drawn due to large scattering of the data points. The transfer length is shown to increase sharply with decreasing sheet resistance (see Fig. 6b). This can be

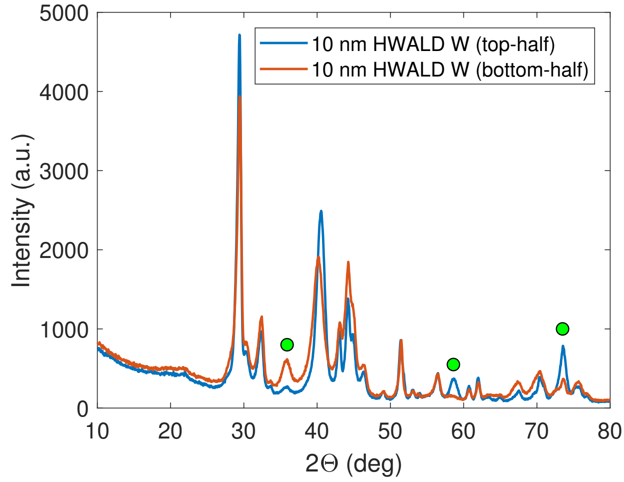

Fig. 5. 2Θ X-ray diffraction measurements for the top- and bottom-half of the 10 nm HWALD W wafer.

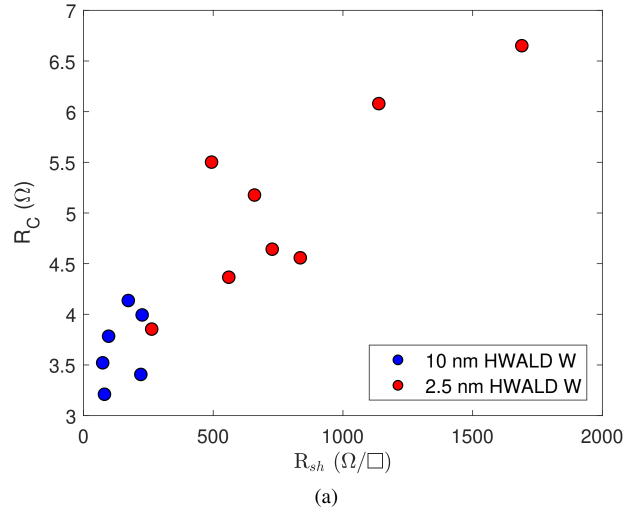

(a)

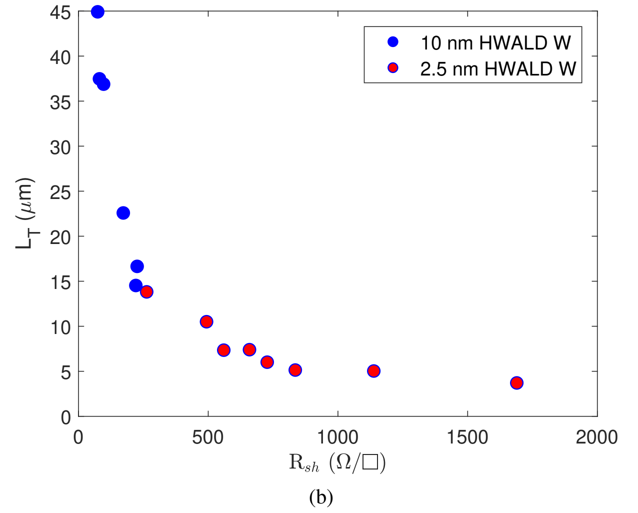

(b)

Fig. 6. The (a) contact resistance and (b) transfer length as a function of the sheet resistance. The blue circles correspond to the structures with the 10 nm W, while the red circles represent the structures having the 2.5 nm film.

explained by the relative change of the magnitude of R_{sh} with respect to the resistance of the electrodes. For higher R_{sh}, the current will be transferred between electrode and sheet over a shorter length scale near the edge of the electrode, thereby taking the least resistance path.

C. Temperature coefficient of resistance

The temperature coefficient of resistance (TCR) was obtained from Van der Pauw structures. Standard sheet resistance measurements were performed at temperatures ranging from -60 to +200 °C. The current-voltage (IV) measurements of a selected structure are shown in Fig. 7a. The negative bias range is largely excluded from the plot, to better visualize the change in R_{sh} with temperature. Fig. 7b and 7c show the evolution of R_{sh} as a function of temperature for structures with differently-thick W films. The magnitude of the TCR is determined by TCR = $1/R_{sh,T=0°C} \times (\Delta R_{sh}/\Delta T)$, where ΔR_{sh} is the change in R_{sh} due to a change in temperature ΔT and $R_{sh,T=0°C}$ is R_{sh} measured at $T = 0°C$. The TCR values change from positive to negative with decreasing the film thickness from 10 to 1 nm. Metals normally exhibit a positive TCR, which is explained by increased phonon scattering at elevated temperatures [35]. The observed negative TCR of the thinnest films can be attributed to for example the dominant hopping-type conductance in the percolated but still not-fully-closed W film [36]. Fig. 8 gives an overview of the measured TCR for structures with various film thicknesses. It can be seen that the 2.5 nm layer corresponds to the transition region; for this film the TCR is small and can be either positive or negative (significant variations observed across the wafer). The largest TCR of $1.1 \cdot 10^{-3}$, measured on a 10-nm-thick structure, is still significantly smaller than the value of the TCR for bulk W (4.5 $\cdot 10^{-3}$, [37]). It shows that thin-film effects already play a role for this thickness, though not dominantly.

D. Field effect

The field effect (FE) measurements were conducted by applying a constant current bias (0.1 - 10 μA) between two adjacent Van der Pauw terminals, while measuring the voltage difference between the other two terminals as a function of the voltage (V_g, swept from -10 V to 10 V and back) applied to the back gate. This allowed to monitor the R_{sh} modulation as a function of the back-gate electric field. Fig. 9a gives an example of such a R_{sh}-V_g dependence, showing a little hysteresis. The FE (in V^{-1}) was defined accordingly to FE = $1/R_{sh}(V_g = 0) \times (\Delta R_{sh}/V_g)$, where the ΔR_{sh} represents the corresponding change of R_{sh} due to the applied V_g, and $R_{sh}(V_g=0)$ is R_{sh} measured at zero V_g. Fig. 9b gives an overview of all FE measurements that were conducted. One can see that the FE increases with increasing sheet resistance. This is expected as the higher R_{sh} can be directly related

to the lower electron concentration. The devices with the lowest sheet resistance exhibit near zero FE. The largest field effect observed at $\sim$4.6$\cdot 10^{-4}$ V^{-1} is of typical magnitude for metals [5-10]. The temperature dependence of the field effect has also been investigated. Fig. 9c shows the results of FE measurements on six different structures at temperatures ranging between 40 and 160 °C. No clear dependence of the FE on temperature has been observed.

V. CONCLUSIONS

In this paper, for the first time to the best of our knowledge, we measured the $R_s h$, R_C, L_T, TCR and FE of 1-10 nm thick tungsten films grown by the novel Hot Wire assisted ALD technique. From fundamental point of view, this is important for exploring the impact of film thickness on film's electrical behavior, whereas practically this knowledge is crucial for the existing and foreseen applications. Especially the remarkable transition from positive to negative TCR around 2.5 nm layer thickness and the observed field effect with a magnitude typical for metals, stand out.

REFERENCES

[1] O. Sneh, R.B. Clark-Phelps, A.R. Londergan, J. Winkler, and T.E. Seidel, "Thin film atomic layer deposition equipment for semiconductor processing", Thin Solid Films, Volume 402, Issues 1-2, pp. 248-261, 2002.

[2] A. Paranjpe, S. Gopinath, T. Omstead, R. Bubber, "Atomic Layer Deposition of AlO_x for Thin Film Head Gap Applications", Journal of the Electrochemical Society, Volume 148, Issue 9, pp. G465-G471, 2001.

[3] T. Luoh, C.-T. Su, T.-H. Yang, K.-C. Chen, C.-Y. Lu, "Advanced tungsten plug process for beyond nanometer technology", Microelectronic Engineering, Volume 85, Issue 8, pp. 1739-1747, 2008.

[4] F. Papadatos et al, "Low resistivity tungsten for 32 nm node MOL contacts and beyond", Microelectronic Engineering, Volume 92, pp. 123-125, 2012.

[5] H.L. Stadler, "Changing Properties of Metals by Ferroelectric Polarization Charging", Physical Revies Letters, Volume 14, Issue 24, pp. 979-981, 1965.

[6] H.J. Juretschke, "Influence of the surface scattering of electrons on the metallic field effect in thin layers", Surface Science, Volume 5, Issue 1, pp. 111-119, 1966.

[7] E.C. McIrvine, "Influence of boundary scattering on the metallic field effect", Surface Science, Volume 5, Issue 2, pp. 171-178, 1966.

[8] A. Berman and H.J. Juretschke, "Origin of the electric field effect in silver", Applied Physics Letters, Volume 18, Issue 10, pp. 417-418, 1971.

[9] R. Dimmich and F. Warkusz, "A simple model of the electric field effect in thin metallic films", Thin Solid Films, Volume 79, Issue 2, pp. 173-184, 1981.

[10] R. Dimmich and F. Warkusz, "The metallic field effect in thin polycrystalline films", Thin Solid Films, Volume 135, Issue 1, pp. 43-50, 1986.

[11] S.M. George, "Atomic layer deposition: an overview", Chemical reviews, vol. 110, pp. 111-131, 2009.

[12] B.S. Lim, A. Rahtu and R.G. Gordon, "Atomic layer deposition of transition metals", Nature Materials, Volume 2, Issue 11, pp. 749-754, 2003.

[13] V.V. Afanas'ev, J.M.M. de Nijs, P. Balk and A. Stesmans, "Degradiation of thermal oxide of the Si/SiO_2/Al system due to vacuum ultraviolet irradiation", Journal of Applied Physics, Volume 78, Issue 11, pp. 6481-6490, 1995.

[14] A.Y. Kovalgin, M. Yang, S. Banerjee, R.O. Apaydin, A.A.I. Aarnink, S. Kinge, and R.A.M. Wolters, "Hot-Wire Assisted ALD: A Study Powered by In Situ Spectroscopic Ellipsometry, Advanced Materials Interfaces, Volume 4, Issue 18, 1700058, 2017.

[15] M. Yang, A.A.I. Aarnink, A.Y. Kovalgin, R.A.M. Wolters and J. Schmitz, "Hot-wire assisted ALD of tungsten films: In-situ study of the interplay between CVD, etching, and ALD modes", Physica Status Solidi (A) Applications and Materials Science, Volume 212, Issue 7, pp. 1607-1614, 2015.

[16] M. Yang, A.A.I. Aarnink, A.Y. Kovalgin, D.J. Gravesteijn, R.A.M. Wolters and J. Schmitz, "Comparison of tungsten films grown by CVD and hot-wire assisted atomic layer deposition in a cold-wall reactor", Journal of Vacuum Science and Technology A: Vacuum, Surfaces and Films, Volume 34, Issue 1, 01A129, 2016.

[17] M. Yang, A.A.I. Aarnink, R.A.M. Wolters, J. Schmitz and A.Y. Kovalgin, "Effects of oxygen, nitrogen and fluorine on the crystallinity of tungsten by hot-wire assisted ALD", ECS Journal of Solid State Science and Technology, Volume 6, Issue 12, pp. P839-P844, 2017.

[18] M. Yang, A.A.I. Aarnink, J. Schmitz and A.Y. Kovalgin, "Low-resistivity α-phase tungsten films grown by hot-wire assisted atomic layer deposition in high-aspect-ratio structures", Thin Solid Films, Volume 646, pp. 199-208, 2018.

[19] M. Yang, A.A.I. Aarnink, J. Schmitz and A.Y. Kovalgin, "Inherently area-selective hot-wire assited atomic layer deposition of tungsten films", Thin Solid Films, Volume 649, pp. 17-23, 2018.

[20] L.J. van der Pauw, "A method of measuring specific resistivity and Hall effect of discs of arbitrary shape", Philips Research Reports, vol. 13, no. 1, pp. 1-9, 1958.

[21] L.J. van der Pauw, "A method of measuring the resistivity and Hall coefficient on lamellae of arbitrary shape", Philips Technical Review, vol. 20, no. 8, pp. 220-224, 1958/59.

[22] W. Versnel, "Analysis of symmetrical Van der Pauw structures with finite contacts", Solid-State Electronics, Volume 21, pp. 1261-1268, 1978.

[23] A.J. Willis and A.P. Botha, "Investigation of ring structures for metal-semiconductor contact resistance determination", Thin Solid Films, vol. 146, pp. 15-20, 1987.

[24] J.H. Klootwijk and C.E. Timmering, "Merits and limitations of circular TLM structures for contact resistance determination for novel III-V hbts", Proc. IEEE 2004 Int. Conference on Microelectronic Test Structures, vol. 17, pp. 247-252, 2004.

[25] G.S. Marlow and M.B. Das, "The effects of contact size and non-zero metal resistance on the determination of specific contact resistance", Solid-State Electronics, Volume 25, Issue 2, pp. 91-94, 1982.

[26] M. Ahmad and B.M. Arora, "Investigation of augeni contacts using rectangular and circular transmission line model", Solid-State Electronics, Volume 35, Issue 10, pp. 1441-1445, 1992.

[27] H. Van Bui, A.Y. Kovalgin, J. Schmitz, and R.A.M. Wolters, APPLIED PHYSICS LETTERS, Volume 103, Issue 5, pp. 051904, 2013.

[28] F. Allen, O. Kennard, D. Watson, L. Brammer, A. Orpen, and R. Taylor, International Tables for Crystallography (Kluwer Academic, Dordrecht 1995), Vol. C.

[29] E. Lassner and W.D. Schubert, Tungsten: Properties, Chemistry, Technology of the Elements, Alloys, and Chemical Compounds (Springer Science & Business Media, New York, 1999).

[30] A. Bartl, "Fundamentals of NS-tungsten powder manufacture", Pd.D. thesis (TU Vienna, 1997).

[31] R.A. Serway, Principles of physics (2nd ed.), Fort Worth, Texas; London: Saunders College Pub. p.602

[32] P.M. Petroff, T.T. Sheng, A.K. Sinha, G.A. Rozgonyi, and F.B. Alexander, "Microstructure, growth, resistivity, and stresses in thin tungsten films deposited by rf sputtering", Journal of Applied Physics, Volume 44, pp. 2545, 1973.

[33] Q. Hao, W. Chen and G. Xiao, "Beta (β) tungsten thin films: Structure, electron transport, and giant spin Hall effect", Applied Physics Letters, Volume 106, pp. 182403, 2015.

[34] P.M. Petroff and W.A. Reed, "Resistivity behavior and phase transformations in β-W thin films", Thin Solid Films, Volume 21, Issue 1, pp. 73-81, 1974.

[35] N.W. Ashcroft and N.D. Mermin, "Solid State Physics", Harcourt Brace College Pub., New York, 1976.

[36] H. Bottger and V.V. Bryksin, "Hopping conductivity in ordered and disordered solids (I)", Physica status solidi B, Volume 78, Issue 9, pp. 9-56, 1976.

[37] R.A. Serway and J.W. Jewett, Principles of Physics: A Calculus-Based Text (5th ed.), Belmont, CA: Brooks/Cole, 2013

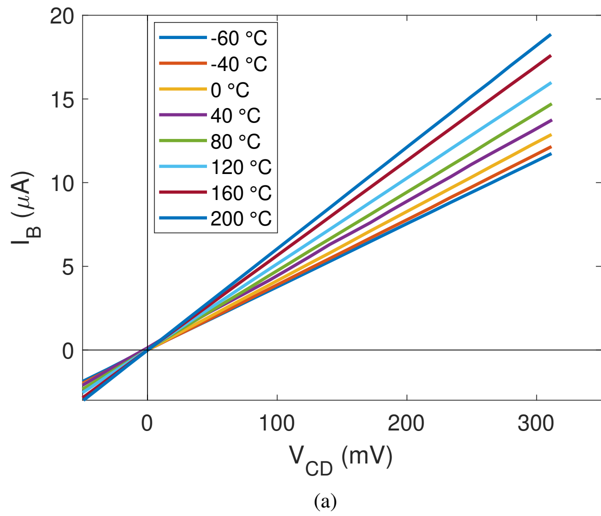

(a)

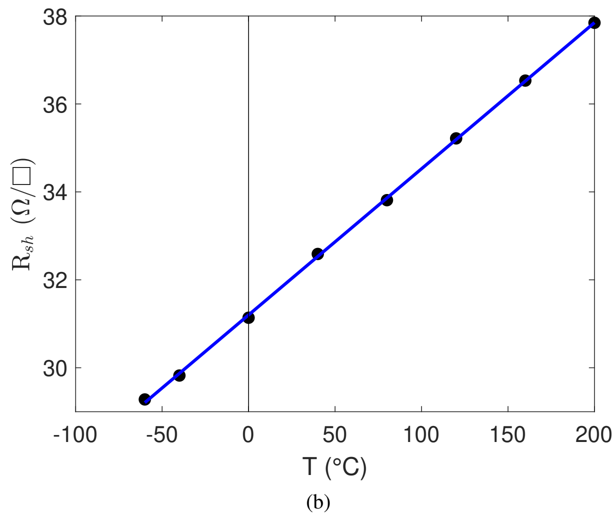

(b)

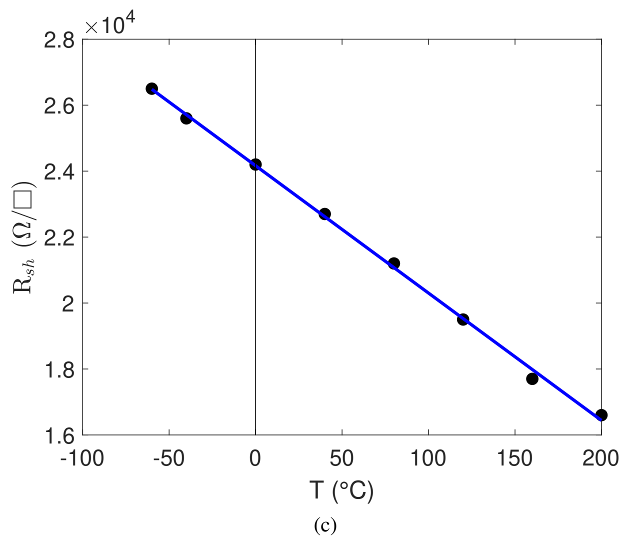

(c)

Fig. 7. Temperature dependent sheet resistance measurements. (a) IV curves of a selected 1.5-nm-thick structure. (b) Sheet resistance of a selected 10-nm-thick structure showing a positive TCR. (c) Sheet resistance of a selected 1.5-nm-thick structure showing a negative TCR.

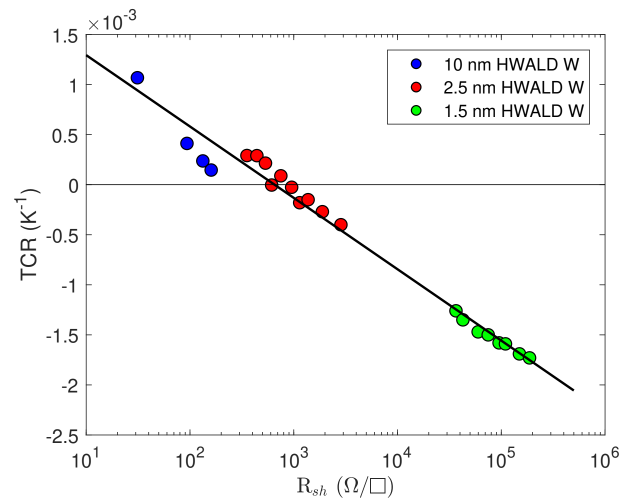

Fig. 8. The cumulative TCR versus sheet resistance plot for various film thicknesses (wafers) and structure positions on each wafer.

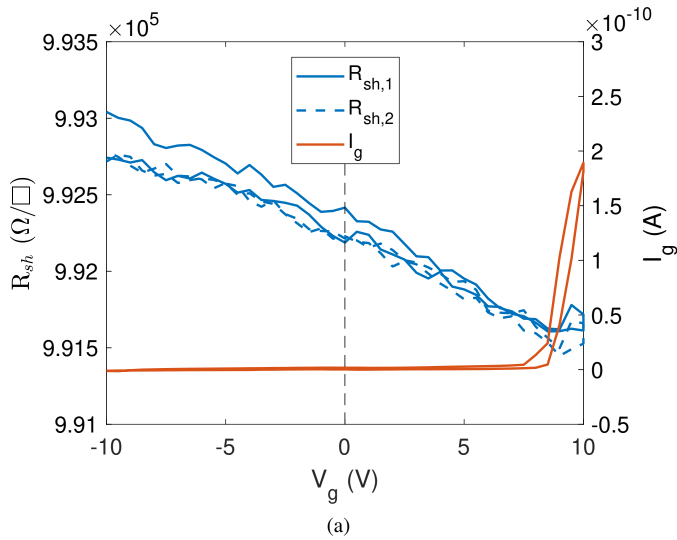

(a)

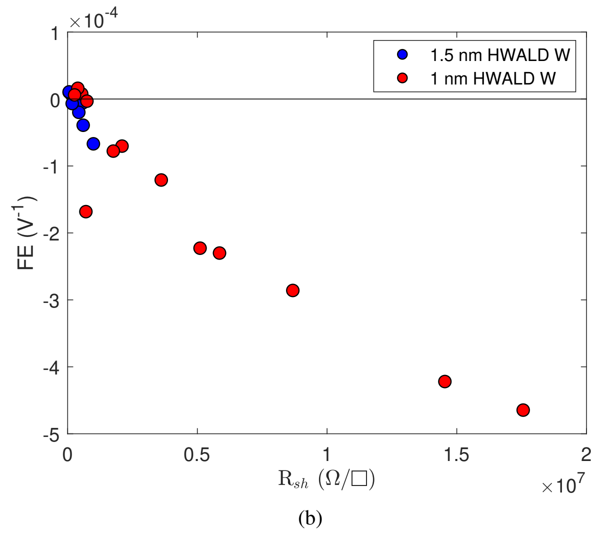

(b)

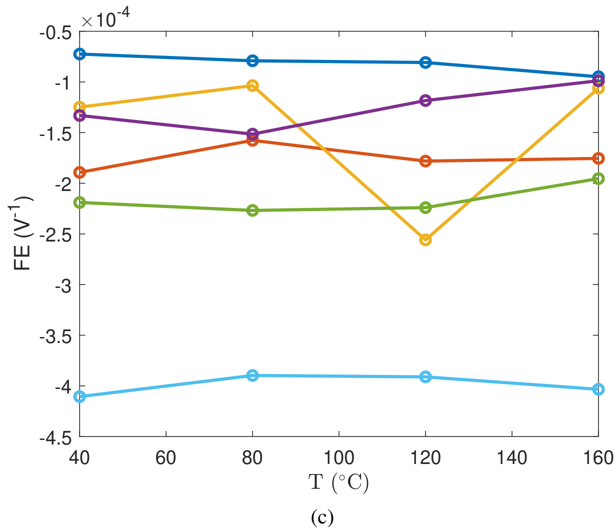

(c)

Fig. 9. (a) The change of the sheet resistance of a selected 1-nm-thick structure while sweeping the back-gate voltage V_g from -10 V to 10 V and backwards; the flat curve with a sharp increase at ∼8 V corresponds to the gate leakage current I_g. (b) The observed field effect as a function of the sheet resistance, for the indicated film thicknesses (wafers) and various structure positions on each wafer. (c) The observed field effect as a function of temperature for various structures.